HHS Public Access

Author manuscript

*Cell*. Author manuscript; available in PMC 2018 June 03.

Published in final edited form as:

*Cell*. 2017 June 01; 169(6): 1090–1104.e13. doi:10.1016/j.cell.2017.04.034.

# Ubiquitination-Deficient Mutations in Human *Piwi* Cause Male Infertility by Impairing Histone-to-Protamine Exchange during Spermiogenesis

**Lan-Tao Gou**[1,7,10], **Jun-Yan Kang**[1,10], **Peng Dai**[1,10], **Xin Wang**[10], **Feng Li**[1,10], **Shuang Zhao**[1], **Man Zhang**[2], **Min-Min Hua**[1,3], **Yi Lu**[3], **Yong Zhu**[4], **Zheng Li**[4], **Hong Chen**[5], **Li-Gang Wu**[1], **Dangsheng Li**[6], **Xiang-Dong Fu**[7], **Jinsong Li**[2,8], **Hui-Juan Shi**[3], and **Mo-Fang Liu**[1,8,9,11]

[1]State Key Laboratory of Molecular Biology, Shanghai Key Laboratory of Molecular Andrology, CAS Center for Excellence in Molecular Cell Science

[2]State Key Laboratory of Cell Biology Shanghai Institute of Biochemistry and Cell Biology, Chinese Academy of Sciences, University of Chinese Academy of Sciences, Shanghai 200031, China

[3]Key Lab of Reproduction Regulation of NPFPC-Shanghai Institute of Planned Parenthood Research, Fudan University Reproduction and Development Institution, Shanghai 200032, China

[4]Department of Andrology and PFD, Center for Men's Health, Department of ART, Institute of Urology, Urologic Medical Center Shanghai General Hospital, Shanghai Key Lab of Reproductive Medicine Shanghai Jiao Tong University, Shanghai, 200080, China

[5]Department of Anatomy, Histology and Embryology, School of Basic Medical Sciences, Fudan University, Shanghai 200032, China

[6]Shanghai Information Center for Life Sciences, Shanghai Institutes for Biological Sciences, Chinese Academy of Sciences, Shanghai 200031, China

[7]Department of Cellular and Molecular Medicine, University of California, San Diego, La Jolla, CA 92093-0651, USA

[8]School of Life Science and Technology, Shanghai Tech University, Shanghai 201210, China

[9]Collaborative Innovation Center of Genetics and Development, Fudan University, Shanghai 200438, China

## Summary

Correspondence to: Hui-Juan Shi; Mo-Fang Liu.

[10]These authors contributed equally

[11]Lead Contact

Supplemental Information: Supplemental Information includes seven figures, three tables, and four movies and can be found with this article online at http://dx.doi.org/10.1016/j.cell.2017.04.034.

**Author Contributions**: M.-F.L. and H.-J.S. planned the project. L.-T.G., J.-Y.K., P.D., X.W., F.L., H.C., L.-G.W., J.L., X.-D.F., H.-J.S., and M.-F.L. designed the experiments. L.-T.G., J.-Y.K., P.D., X.W., F.L., S.Z., M.Z., M.-M.H., and Y.L. conducted the experiments. Y.Z., Z.L., and H.-J.S. provided human specimens. L.-T.G., J.-Y.K., P.D., X.W., F.L., S.Z., and M.-F.L. analyzed the data. L.-T.G., J.-Y.K., D.L., X.-D.F., and M.-F.L. wrote the paper. All authors discussed the results and commented on the manuscript. M.-F.L. supervised the overall work and H.-J.S. was responsible for clinical studies.

Genetic studies have elucidated critical roles of Piwi proteins in germline development in animals, but whether *Piwi* is an actual disease gene in human infertility remains unknown. We report germline mutations in human *Piwi* (*Hiwi*) in patients with azoospermia that prevent its ubiquitination and degradation. By modeling such mutations in *Piwi* (*Miwi*) knockin mice, we demonstrate that the genetic defects are directly responsible for male infertility. Mechanistically, we show that MIWI binds the histone ubiquitin ligase RNF8 in a Piwi-interacting RNA (piRNA)-independent manner, and MIWI stabilization sequesters RNF8 in the cytoplasm of late spermatids. The resulting aberrant sperm show histone retention, abnormal morphology, and severely compromised activity, which can be functionally rescued via blocking RNF8-MIWI interaction in spermatids with an RNF8-N peptide. Collectively, our findings identify *Piwi* as a factor in human infertility and reveal its role in regulating the histone-to-protamine exchange during spermiogenesis.

## Graphical abstract

Male infertility in mice and humans can result from mutations that stabilize the Piwi protein in late spermatids: sperm defects are due to aberrant histone retention, not piRNA misregulation.

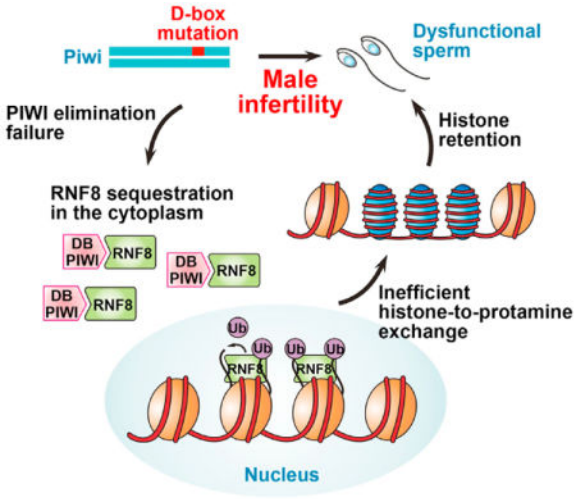


## Introduction

Genomic DNA is organized on histone octamer in the nucleus of typical eukaryotic cells but is alternatively packaged on protamines in sperm of many animals (Kornberg and Thomas, 1974; Oliva, 2006; Balhorn, 2007). Protamines are small, highly basic proteins that promote a much higher degree of DNA condensation to facilitate the packaging of genomic DNA into tiny sperm heads, which is essential to produce functional sperm (Oliva, 2006). Such histone-to-protamine exchange is a complex process, which occurs during post-meiotic male germ cell development, known as spermiogenesis, when haploid round spermatids elongate and transform into spermatozoa (Meistrich et al., 2003; Oliva, 2006). Despite the discovery of protamines in animal sperm more than a century ago and the well-established linkage between defective histone-to-protamine transition and male infertility in mammals (Meistrich et al., 2003; Oliva, 2006; Yan, 2009), little is known about the regulatory

mechanism that governs this transition. A recent study suggests that global ubiquitination of H2A and H2B mediated by the ubiquitin ligase RNF8 is a key initial step in this process (Lu et al., 2010), but how this transition is triggered at a defined developmental stage of spermatogenesis remains unknown.

The evolutionarily conserved Piwi proteins belong to the Piwi clade of the Argonaute family, each of which is specifically expressed during the development of animal germline (Juliano et al., 2011; Siomi et al., 2011). Piwi proteins are known to enlist germline-specific Piwi-interacting RNAs (piRNAs) to suppress transposable elements and protect the integrity of the genome in germ cells (Juliano et al., 2011; Siomi et al., 2011). We and others recently showed that the Piwi/piRNA machinery also functions in regulating protein coding genes in germ cells (Gou et al., 2014; Zhang et al., 2015; Barckmann et al., 2015; Watanabe et al., 2015; Vourekas et al., 2016). Extensive genetic studies in worms, flies, fish, and mice indicate that Piwi proteins are essential for gametogenesis in animals (Cox et al., 1998; Harris and Macdonald, 2001; Deng and Lin, 2002; Kuramochi-Miyagawa et al., 2004; Carmell et al., 2007; Houwing et al., 2008; Batista et al., 2008). For instance, all three *Drosophila* Piwi proteins, including Argonaute 3, Aubergine, and PIWI, are required for germ cell formation and germline stem cell maintenance in both male and female flies, consistent with their expression in testis and ovary (Cox et al., 1998; Harris and Macdonald, 2001). The mouse genome encodes three *Piwi* paralogs, *Miwi*, *Mili*, and *Miwi2*, all of which are highly expressed in the testis, and accordingly, all are required for male but not female fertility (Deng and Lin, 2002; Kuramochi-Miyagawa et al., 2004; Carmell et al., 2007).

Piwi proteins consist of four distinct domains: the N-terminal, PAZ, MID, and PIWI domains (Meister, 2013). The PAZ and MID domains are responsible for piRNA loading whereas the PIWI domain resembles RNase H (De Fazio et al., 2011; Reuter et al., 2011; Cora et al., 2014), but the functional significance of the N-terminal domain has been unclear. We recently identified a conserved destruction box (D-box), a signature shared by the substrates of the APC/C ubiquitin E3 ligase, in the N-terminal domain of vertebrate PIWI proteins, including MIWI in mice and HIWI in humans (Zhao et al., 2013). We further demonstrated that MIWI is ubiquitinated and degraded by APC/C in a D-box-dependent manner in late spermiogenesis in mice (Zhao et al., 2013). By testis transduction, we provided initial evidence that this MIWI elimination is critical for proper transformation of spermatids into spermatozoa.

The human genome encodes four *Piwi* family members, including *Hiwi*, *Hili*, *Hiwi2*, and *Piwil3* (Sasaki et al., 2003), all of which are mainly expressed in testis, but their potential function in human germline development has remained elusive. Despite the identification of several single nucleotide polymorphisms (SNPs) in human *Piwi* genes (Gu et al., 2010), the functional significance, if any, of such SNPs has remained unclear. Suspecting that HIWI D-box element might be a hotspot for mutations that cause male infertility in humans, we embarked on a screening effort to sequence the D-box region spanning the sixth and seventh exons of the *Hiwi* gene in a group of 413 patients with idiopathic azoospermia, which led to the identification of specific D-box mutations in three patients with azoospermia, including R218A/L221A (Patient 1), L221G/N225H (Patient 2), and L221R (Patient 3). By modeling such mutations in both knockin and trans-genic mice, we demonstrate that D-box mutations

impeded MIWI degradation and contribute to male infertility. Mechanistically, we find that the MIWI D-box mutations in male mice impair the histone ubiquitination and histone-to-protamine transition during spermiogenesis, reminiscent of the phenotype observed in the histone ubiquitin ligase RNF8-deficient mice (Lu et al., 2010). We further demonstrate that MIWI binds RNF8 in the cytoplasm of earlier spermatids, and MIWI degradation by APC/C in late spermatids is required for nuclear translocation of RNF8 to catalyze histone ubiquitination and trigger histone removal. These findings highlight a piRNA-independent function of HIWI/MIWI in late stage germline cells and demonstrate that defects in this regulatory pathway are implicated in infertility in males.

## Results

### *Hiwi* D-Box Mutations in Patients with Azoospermia

To explore the functional importance of regulated PIWI ubiquitination by APC/C in human spermatogenesis, we screened for potential mutations in the D-box element of *Hiwi* in a cohort of 413 patients with idiopathic azoospermia and 300 fertile controls (Figure 1A). All patients underwent semen analyses at least on three different occasions, and those with a history of or-chitis, obstruction of vas deferens, or endocrine disorders were excluded. All the fertile controls had fathered at least one child. By sequencing the D-box region spanning the sixth and seventh exons of the *Hiwi* gene (Figure 1B, upper panel), we identified several heterozygous mutations in three patients, including R218A/L221A (Patient 1), L221G/N225H (Patient 2), and L221R (Patient 3), but none in controls (Figures 1B and 1C). By full-length sequencing, we confirmed that these mutations are the only changes that cause amino acid substitutions in the *Hiwi* gene in these patients. Consistent with our previous results (Zhao et al., 2013), all of these newly identified D-box mutations severely impaired HIWI ubiquitination without affecting its piRNA-loading or slicer activities (Figure S1).

To track these mutations in patient pedigrees, we sequenced the *Hiwi* D-box region of both parents and siblings of Patients 1 and 2 (we lost the contact with Patient 3 during the investigation). Intriguingly, both parents of Patient 1 have wild-type D-box sequences (Figure 1D, left panel), suggesting R218A/L221A as de novo mutations in this patient. In contrast, the mother of Patient 2 has the same heterozygous L221G/N225H mutations, while both his father and brother (with normal fertility) carry the wild-type D-box (Figure 1D, right panel). These data suggest both de novo and inheritable mutations in the *Hiwi* D-box, the latter of which agrees with previous observations in mice that *Piwi* mutations affecting male fertility could be maternally transmitted (Deng and Lin, 2002; Kuramochi-Miyagawa et al., 2004; Carmell et al., 2007).

### Male Sterility Caused by the MIWI D-Box Mutation in Knockin Mice

To determine whether *Hiwi* D-box mutations play a causative role in male infertility, we constructed a conditional knockin mouse with R218A/L221A mutations in the *Miwi* gene (referred to as $Miwi^{DB}$), mimicking those identified in Patient 1 (Figures 2A and S2A). By crossing $Miwi^{DB}$ mice to a primordial germ cell (PGC)-specific TNAP-Cre transgenic mouse (Lomelí et al., 2000), we obtained heterozygous germline-specific R218A/L221A knockin mice ($Miwi^{+/DB}$-*Cre*; Figure S2B). Strikingly, all tested $Miwi^{+/DB}$-*Cre* males were

sterile (Figure 2B), while all *Miwi*$^{+/DB}$-*Cre* females exhibited normal fertility. By recapitulating the disease phenotype in a mouse model, these results suggest that the original mutations are likely disease drivers in the humans, although we could not rule out other potential modifiers in the patient's genome that may help manifest the disease phenotype.

We next asked at which stage spermatogenesis failed in *Miwi*$^{+/DB}$-*Cre* mice. We found that the average weight of testes from adult *Miwi*$^{+/DB}$-*Cre* mice was ~25% lower than that of controls (*Miwi*$^{+/DB}$) (Figure S2C), but detected no significant change in the numbers of tubules per testis cross-section and Sertoli cells per tubule cross-section in *Miwi*$^{+/DB}$-*Cre* testes (Figures S2D and S2E). Compared to *Miwi*$^{+/DB}$ controls, spermatocytes, round spermatids, and early elongating spermatids were largely unaltered, while condensed spermatids at steps 14–16 (stages IV–VI, VII, and VIII) were strongly reduced in the seminiferous tubules of *Miwi*$^{+/DB}$-*Cre* testes (Figures 2C and 2D), concomitant with apoptotic signals detected in late spermatids (Figure S2F). This differs from the phenotypes of *Miwi* null or slicer-dead mutant mice where spermatogenesis is arrested at early round spermatids after meiosis (Deng and Lin, 2002; Reuter et al., 2011). Thus, the D-box mutations caused defective spermatogenesis at a later spermiogenic stage in *Miwi*$^{+/DB}$-*Cre* mice. Further analyses showed reduction of ub-MIWI conjugates (Figure S2G) and elevation of the MIWI protein level in *Miwi* $^{+/DB}$-*Cre* late spermatids compared to *Miwi*$^{+/DB}$ controls (Figures 2E and S2H).

## MIWI Stabilization in Late Spermatids Is Sufficient to Cause Male Sterility

Because we showed earlier that APC/C-mediated MIWI degradation occurs in late spermatids (Zhao et al., 2013), we then tested whether MIWI stabilization in the spermiogenic phase is sufficient to cause the disease phenotype. To this end, we generated transgenic mice expressing either wild-type (WT/Tg: *Prm*-Flag-MIWI-IRES-GFP) or D-box mutant MIWI (DB/Tg: *Prm*-D-box mutant [R218A/L221A] MIWI-IRES-GFP) driven by the haploid spermatid-specific *Protamine 1* promoter (*Prm*) and obtained two male founders for each transgene. As expected, both DB/Tg males were sterile, while the WT/Tg males displayed normal fertility (Figure S3A). We confirmed that all transgenes were specifically expressed in testes (Figure S3B), with similar copy numbers and mRNA levels (Figures S3C and S3D). Importantly, immunostaining and western blotting indicated that, while both wild-type and mutant MIWI proteins were efficiently expressed in haploid spermatids in these transgenic males, only the mutant protein became accumulated in late spermatids (Figures S3E and S3F). Notably, the testes of the DB/Tg males were substantially smaller than those of WT/Tg or non-transgenic males (Figure S3G). Histological analyses indicated nearly complete absence of elongated spermatids (Figure S3H), and TUNEL assay revealed extensive apoptosis in late spermatids (Figure S3I) in DB/Tg testes. These results demonstrated that selective stabilization of MIWI in late spermatids is sufficient to severely impair spermatid development.

Intriguingly, we noted that DB/Tg males suffered from more severe spermiogenesis defects than *Miwi*$^{+/DB}$-*Cre* males. We observed little spermatozoa in the epididymides of DB/Tg males (Figure S3J), but clearly detectable spermatozoa in *Miwi*$^{+/DB}$-*Cre* males, despite dramatically reduced sperm count in their epididymides relative to *Miwi*$^{+/DB}$ controls

(Figures 3A and 3B). The more severe azoospermia-like phenotype in DB/Tg males likely resulted from much higher amount of mutant MIWI in transgenic mice than in the knockin mice (Figure S3K). If MIWI impedes sperm development in a dosage-dependent manner, we would expect more *Miwi*$^{+}$ sperm than *Miwi*$^{DB}$ sperm in *Miwi*$^{+/DB}$-*Cre* males, given that *Miwi* is still transcribed in haploid round spermatids. Indeed, sequencing epididymal sperm genomic DNA in the *Miwi* D-box region revealed an ~2:1 ratio of *Miwi*$^{+}$:*Miwi*$^{DB}$ genotype in sperm from adult *Miwi*$^{+/DB}$-*Cre* males (Figure S4A). These data demonstrated that the levels of the mutant MIWI protein correlate to the degree of developmental defects in spermatids.

## Abnormal Chromatin Compaction in *Miwi*$^{+/DB}$-*Cre* Sperm

Because *Miwi*$^{+/DB}$-*Cre* mice were still capable of producing some sperm, we characterized the functionality of these sperm. Remarkably, computation-assisted semen analyses (CASA) indicated little movement and forward progression of sperm from *Miwi*$^{+/DB}$-*Cre* mice (Figure 3C), and in vitro fertilization (IVF) showed that those sperm barely fertilized wild-type oocytes (Figure S4B). Therefore, in addition to the reduction in number, the functionality of *Miwi*$^{+/DB}$-*Cre* sperm was also compromised. To understand the cause of nonfunctional sperm from *Miwi*$^{+/DB}$-*Cre* males, we next examined the genome integrity by intracytoplasmic sperm injection (ICSI). We found that 7 out of 36 oocytes that survived the injection of *Miwi*$^{+/DB}$-*Cre* sperm nuclei successfully developed into blastocysts, a rate comparable to that obtained with control sperm nuclei from *Miwi*$^{+/DB}$ males (21 blastocysts from 98 survived oocytes) (Figure S4B). Importantly, both *Miwi*$^{+}$ and *Miwi*$^{DB}$ sperm could fertilize oocytes in ICSI to produce blastocysts as expected (Figure S4C), indicating that *Miwi*$^{+/DB}$-*Cre* sperm maintain the genome integrity required to fertilize oocytes and support embryonic development.

We further inspected the sperm morphology under both differential interference contrast (DIC) and scanning electron microscopes. The majority of *Miwi*$^{+/DB}$-*Cre* sperm showed abnormally curved back heads (Figure 3D, right panel). Moreover, their nuclei were more efficiently stained with acidic aniline (Figure 3E), indicative of less condensed chromatin in these sperm. Indeed, transmission electron microscopy confirmed that most of sperm heads in *Miwi*$^{+/DB}$-*Cre* epididymal sections were less condensed compared with *Miwi*$^{+/DB}$ controls (Figure 3F). These observations pointed to defective chromatin compaction in sperm produced by *Miwi*$^{+/DB}$-*Cre* males.

## Impaired Histone-to-Protamine Exchange in *Miwi*$^{+/DB}$-*Cre* Mice

To investigate the potential cause(s) underlying abnormal chromatin condensation in *Miwi*$^{+/DB}$-*Cre* sperm, we first examined the transcriptome and piRNA levels in *Miwi*$^{+/DB}$-*Cre* elongating spermatids. We found insignificant differences in the transcriptome, despite some changes above the statistical cutoff (Figure S4D; Table S1) and in the levels of total testicular piRNAs and MIWI-associated piRNAs, between knockin and control mice (Figures S4E and S4F). These data suggest that the D-box mutations do not significantly affect gene expression in late spermatids and piRNA biogenesis in testes.

We next performed proteomic analysis of *Miwi*$^{+/DB}$-*Cre* sperm and identified 19 proteins that were significantly upregulated (>3-fold) relative to *Miwi*$^{+/DB}$ controls (Table S2). In particular, the levels of histones H2A, H2B, H3, H4, and their variants were greatly elevated in *Miwi*$^{+/DB}$-*Cre* sperm. Immunostaining and western blotting verified abnormal retention of all core histones with the most dramatic increase in H2B, and conversely, moderately reduced levels of protamines PRM1 and PRM2 in *Miwi*$^{+/DB}$-*Cre* sperm compared to *Miwi*$^{+/DB}$ controls (Figures 4A and 4B; Table S2). Further global analysis confirmed significant elevation of nucleosomes in *Miwi*$^{+/DB}$-*Cre* sperm relative to both wild-type and *Miwi*$^{+/DB}$ controls (data not shown). Given that most nucleosomal histones are initially replaced by transition proteins and subsequently by protamines during spermio-genesis (Meistrich et al., 2003; Oliva, 2006), we further asked whether there is a defect in the incorporation of the transition proteins and protamines into chromatin in *Miwi*$^{+/DB}$-*Cre* elongating spermatids in which the histone-to-protamine exchange has initiated. Western blotting showed a significant decrease of TNP1, PRM1, and PRM2 proteins on chromatin along with an increase of TNP1 in soluble fractions of *Miwi*$^{+/DB}$-*Cre* elongating spermatids (Figure 4C), indicating impaired histone-to-protamine exchange in *Miwi*$^{+/DB}$-*Cre* mice. Because the histone-to-protamine exchange is essential for producing functional sperm (Braun, 2001), these results suggest that an incomplete histone-to-protamine exchange may underlie the functional defect of *Miwi*$^{+/DB}$-*Cre* sperm.

## Decreased Histone Ubiquitination in *Miwi*$^{+/DB}$-*Cre* Late Spermatids

We proceeded to investigate the molecular basis for impaired histone-to-protamine exchange during spermiogenesis in *Miwi*$^{+/DB}$-*Cre* mice. A previous report suggests that ubiquitination of H2A and H2B in elongating spermatids is an early step in triggering global nucleosome removal in the mouse (Lu et al., 2010), but how this process is regulated in a defined developmental stage has remained unclear. We thus examined the levels of ubiquitinated H2A and H2B in late spermatids enriched from adult *Miwi*$^{+/DB}$-*Cre* mice. By western blotting, we observed a marked decrease in both H2A ubiquitination (ub-H2A) and H2B ubiquitination (ub-H2B) in these cells in comparison with *Miwi*$^{+/DB}$ controls (Figure 5A). Immunostaining further confirmed significant reduction of ub-H2B in elongating spermatids from *Miwi*$^{+/DB}$-*Cre* testes (Figure 5B, left). Consistently, the level of H4K16ac, a downstream event of ub-H2B, was also significantly decreased in *Miwi*$^{+/DB}$-*Cre* late spermatids (Figures 5A and 5B, right). These results, coupled with MIWI accumulation in late spermatids (Figures 2E and S2H), led us to hypothesize that MIWI ubiquitination and subsequent elimination might be a trigger signal for histone ubiquitination and removal in late spermatids. To directly test this, we knocked down *Miwi* through testis transduction in *Miwi*$^{+/DB}$-*Cre* males with a lentiviral *shMiwi*:GFP vector as we described earlier (Gou et al., 2014). Western blotting of sorted GFP$^{+}$ late spermatids indeed revealed an elevated ub-H2B level in MIWI knockdown late spermatids (Figure 5C, lane 4). This result formally pointed to the possibility that MIWI might somehow repress H2B ubiquitination in late spermatids.

## MIWI Controls Subcellular Localization of the Histone Ubiquitin Ligase RNF8 in Spermatids

The RING domain protein RNF8 has been established as the ubiquitin E3 ligase for histone ubiquitination in mouse spermatids, which is responsible for histone-to-protamine exchange

(Lu et al., 2010), but not critical for protamine expression (Sin et al., 2012). More importantly, RNF8-deficient mice resemble our *Miwi*$^{+/DB}$-*Cre* mice in many respects, including male but not female infertility, strong reduction of late spermatids at steps 14–16 and sperm count, less condensed chromatin in sperm, as well as decreased ub-H2A and ub-H2B in late spermatids and severe histone retention in sperm (Lu et al., 2010). Such striking similarity in phenotype between the two mouse models prompted us to test whether MIWI acts through RNF8 to regulate histone ubiquitination.

We found little difference in *Rnf8* expression between *Miwi*$^{+/DB}$-*Cre* and control late spermatids (Figure S5), which excludes the regulation of *Rnf8* expression by MIWI. We then sought to test whether MIWI controls the activity of RNF8. Given that MIWI is present in the cytoplasm of spermatids while RNF8-mediated histone ubiquitination most likely occurs in the nucleus, we examined their subcellular localization in *Miwi*$^{+/DB}$-*Cre* or control spermatids at different developmental stages. Surprisingly, double immunostaining revealed that RNF8 clearly colocalizes with MIWI in cytoplasm of round spermatids (RS) from both control and *Miwi*$^{+/DB}$-*Cre* mice (Figures 5D, left, and S6A). Interestingly, we observed that RNF8 translocates to the nucleus of control late spermatids (LS), which is accompanied by MIWI degradation (Figures 5D, top right, and S6A, top). In contrast, RNF8 failed to enter the nucleus of *Miwi*$^{+/DB}$-*Cre* late spermatids (Figures 5D, bottom right, and S6A, bottom), indicative of stabilized MIWI in sequestering RNF8 in the cytoplasm of late spermatids. To demonstrate that MIWI destabilization acts as a switch for RNF8 nuclear translocation and subsequent histone ubiquitination during normal spermatid development, we knocked down *Miwi* in wild-type round spermatids (RS) by testis transduction of lentiviral *shMiwi*:GFP. Indeed, *Miwi* knockdown led to a partial nuclear translocation of RNF8 in round spermatids, which is accompanied by abnormal H2B ubiquitination in these cells (Figure 5E). Taken together, these results revealed that MIWI sequesters RNF8 in the cytoplasm of round spermatids and MIWI elimination is a prerequisite for RNF8 nuclear translocation in late spermatids.

## MIWI and RNF8 Form a Complex

Next, we sought to understand the mechanism whereby MIWI anchors RNF8 in the cytoplasm. First, we tested whether MIWI physically interacts with RNF8. To this end, we performed co-immunoprecipitation (coIP) to examine potential interaction between MIWI and RNF8. Indeed, we found that Flag-MIWI and Myc-RNF8 were able to pull down each other efficiently in co-transfected 293T cells (Figure S6B). As a control, Flag-MILI showed little interaction with Myc-RNF8 (Figure S6B). We further extended this interaction in the native context by demonstrating that endogenous RNF8 interacted with MIWI in enriched late spermatids (Figure S6C). Notably, anti-RNF8 pulled down much more MIWI protein in *Miwi*$^{+/DB}$-*Cre* late spermatids compared with *Miwi*$^{+/DB}$ controls, likely due to the elevated MIWI levels in *Miwi* $^{+/DB}$-*Cre* late spermatids. By proteomic analysis, we detected multiple peptides of MIWI and RNF8 in both anti-RNF8 and anti-MIWI IPed complexes from mouse spermatids (Table S3). These results support the interaction between MIWI and RNF8 in spermatids.

Having shown MIWI/RNF8 interaction, we wondered whether such interaction functions in modulating the ubiquitin ligase activity of RNF8. To test this, we established an in vitro RNF8 ubiquitination assay using H2B as substrate, as described previously (Mailand et al., 2007), and we made similar observation with H2A (data not shown). Interestingly, both purified Flag-tagged MIWI and its D-box mutant were able to repress H2B ubiquitination in a dosage-dependent manner (Figure 5F, lanes 7–14), and in sharp contrast, Flag-tagged MILI, another mouse Piwi member that does not interact with RNF8 (Figure S6B), showed no detectable impact on these reactions (lanes 15–18). These data strongly suggest that MIWI directly binds and inhibits the ubiquitin ligase activity of RNF8, which may suppress the general activity of RNF8, including its function on other substrates in the cytoplasm. Importantly, we found that the inhibitory effect of MIWI on RNF8 activity was unaltered in the presence of either mouse testicular piRNAs or chemically synthesized 30-nt piR-1 (Figure S7A). Moreover, both piRNA-loading-deficient (Y346/347A) and slicer dead (ADH) MIWI mutant proteins inhibited H2B ubiquitination by RNF8 comparable to wild-type MIWI (Figure S7B). Consistently, co-immunoprecipitation assay showed that the interaction between MIWI and RNF8 was barely affected by mutations that destroyed piRNA-loading or slicer activity in MIWI (Figures S7C and S7D). Together, these results revealed a piRNA-independent function of MIWI in regulating the ubiquitin ligase activity of RNF8.

## RNF8 Requires Its $^{68}$QNPEG$^{72}$ Motif to Bind MIWI

To further dissect the interaction between MIWI and RNF8, we mapped the domain(s) in RNF8 responsible for MIWI binding by testing a series of truncated mutants of RNF8 (critical mutants shown in Figure 6A) using the full-length MIWI in coIP assay. We identified the $^{68}$QNPEG$^{72}$ peptide in the N-terminal domain of RNF8 as an essential motif for MIWI binding. This motif is highly conserved among vertebrates, further supporting its importance. Interestingly, we found that an ~200 aa RNF8 N-terminal peptide (1–210 amino acids; RNF8-N) could substantially interact with MIWI, while substitution of $^{68}$QNPEG$^{72}$ with $^{68}$AAAAA$^{72}$ (RNF8-N$^{mut}$) potently prevented MIWI binding (Figure 6B). Importantly, RNF8-N, but not RNF8-N$^{mut}$, effectively impaired the binding of full-length RNF8 to MIWI in co-transfected 293T cells (Figure 6C). Taking advantage of in vitro RNF8-mediated H2B ubiquitination, we showed that RNF8-N, but not RNF8-N$^{mut}$, substantially relieved the inhibitory effect of MIWI on RNF8 activity (Figure 6D). These results indicate that RNF8-N is able to compete with full-length RNF8 in MIWI binding.

### Functional Rescue of Defective Spermiogenesis in *Miwi*$^{+/DB}$-*Cre* Mice with the RNF8-N Peptide

The RNF8-N peptide that interferes with the MIWI-RNF8 interaction was used next as a tool to test whether RNF8 sequestration by MIWI in the cytoplasm of late spermatids is a key event that causes defective spermiogenesis in *Miwi*$^{+/DB}$-*Cre* mice. We therefore constructed a Myc-tagged RNF8-N-IRES-Cyto IV-fused EGFP lenti-viral vector driven by the spermatid-specific *Prm* promoter to express the RNF8-N peptide (Figure S7E). In this construct, we developed a strategy to track transduced spermatids by fusing a mitochondrial targeting signal (Cyto IV) to EGFP (Cyto IV-EGFP), which is anchored on the mitochondria of sperm, thus allowing us to track the sperm progressed from transduced spermatids. In line

with our in vitro data, we found that endogenous RNF8 was released and translocated to the nucleus of RNF8-N transduced-late spermatids (Figure 7A, left; note that anti-RNF8 antibody targets at the C-terminal domain of RNF8, thus can only stain for endogenous RNF8 in this experiment), but it was still trapped in the cytoplasm of RNF8-$N^{mut}$-transduced cells (Figure 7A, right). As expected, H2B ubiquitination was substantially restored in RNF8-N transduced-late spermatids, but not in RNF8-$N^{mut}$-transduced cells (Figure 7B). Importantly, H2B was barely stained in RNF8-N transduced-sperm, but still readily detectable in RNF8-$N^{mut}$-ransduced sperm (Figure 7C; compare $GFP^+$ sperm I and II with $GFP^-$ sperm III). Moreover, DIC assay revealed that wild-type RNF8-N transduced-sperm, but not RNF8-$N^{mut}$ transduced-sperm, showed morphology close to the wild-type (Figure 7C). These results demonstrated that blocking RNF8-MIWI interaction in mutant late spermatids was able to functionally rescue defective spermiogenesis in *Miwi*$^{+/DB}$-*Cre* mice.

We next asked if the functionality of mutant sperm could be rescued by the RNF8-N peptide. To this end, we examined whether RNF8-N was able to rescue the motility of mutant sperm, a critical criterion of the functional sperm. As expected, unlike active control sperm, *Miwi* $^{+/DB}$-*Cre* sperm showed little mobility (Movies S1 and S2). Interestingly, the $GFP^+$ sperm from RNF8-N-transduced *Miwi*$^{+/DB}$-*Cre* mice (Movie S3), but not those from RNF8-$N^{mut}$-transduced controls (Movie S4), swam actively, indicating that the RNF8-N peptide effectively recovered the mobility of mutant sperm. These results demonstrate that blocking RNF8-MIWI interaction was able to rescue the activity of *Miwi*$^{+/DB}$-*Cre* sperm.

## Discussion

Despite genetic studies on various animal models indicating that Piwi proteins are essential for animal germline development and fertility, the roles of *Piwi* in human genetics have not been demonstrated. In the present study, we identified specific D-box mutations in *Hiwi* from patients with idiopathic azoospermia, and by modeling such mutations in mouse models, we demonstrate their direct contribution to male infertility. More importantly, our data further indicate that MIWI ubiquitination/degradation is coupled with histone ubiquitination during late spermiogenesis, and MIWI stabilization inhibits RNF8 nuclear translocation and RNF8-mediated histone ubiquitination in late spermatids, which in turn cripples the histone-to-protamine transition to cause compromised sperm production both in quantity and quality in *Miwi*$^{+/DB}$-*Cre* males (Figure 7D). Thus, our work identifies a role for Piwi function in human genetics and reveals mechanism for regulated packaging of genomic DNA into functional sperm.

### *Hiwi* Mutations Linked to Human Infertility

Recent studies have advanced our understanding of how piRNAs are processed and how Piwi/piRNAs function in animals (Han et al., 2015; Mohn et al., 2015; Yu et al., 2015; Iwasaki et al., 2015; Tang et al., 2016; Izumi et al., 2016). However, none of these events have been shown to be relevant to human infertility yet. In addition, up to date, none of SNPs in human *Piwi* genes has been definitively linked to any disease. Through screening human patients, we determined the sequence of the D-box region (~1 kb out of 45 kb) of the *Hiwi* gene in an azoospermia patient population and identified three patients with

heterozygous D-box mutations in their *Hiwi* gene. Due to the lack of in vitro cell culture system for dissecting the roles of gene mutations in human male germ cell development, we generated knockin and transgenic mouse models and demonstrated the causative role of D-Box mutations in male sterility, thus establishing a tight functional correspondence between mice and humans.

Due to the complexity of male infertility as a presumably polygenetic trait amended by hundreds of genetic mutations or polymorphisms as well as environmental, lifestyle, or occupational factors (Schultz et al., 2003; Ferlin et al., 2006; Yan, 2009), any specific type of genetic mutations or polymorphisms may not be frequently present in the pool of patients suffering male infertility. We noted a recent finding of *Wt1* mutations in azoospermia, in which six missense mutations were detected in the full-length *Wt1* gene among 529 human patients (Wang et al., 2013), a mutation rate comparable to that in our study. The available genome-wide association study (GWAS) on human male infertility are based on SNP arrays and none of the array probes covered the D-box region in *Hiwi* (Gu et al., 2010; Hu et al., 2012). Future exome sequencing of male infertile patient DNA samples will be required to further evaluate the existence and frequency of potential mutations in *Hiwi* as well as other genes in the piRNA system in this context. Given our small sample size, we also note that it is possible that other potential modifiers in the patient may contribute to the disease phenotype.

### Dominant Effects of *Miwi* D-Box Mutations on Male Infertility

We noted that all three identified infertile patients carry one wild-type *Hiwi* and one mutant allele. Intriguingly, unlike most infertile mutations that show sterile phenotype only in homozygous state and/or even in combination with other gene mutations, *Miwi* D-box mutations in heterozygous state show complete penetrance in causing male sterility. These mice express both wild-type MIWI and D-box mutant proteins, but wild-type protein is ubiquitinated and degraded by APC/C during late spermiogenesis, while the mutant protein becomes accumulated, leading to impaired spermiogenesis. We have further verified this dominant infertile effect by using transgenic mice to exogenously express D-box mutant MIWI in post-meiotic spermatids. The transgenic mice show even more severe spermiogenic defects, most likely due to higher mutant MIWI expression than those in knockin mice. Consistently, the heterozygous knockin mice generate more wild-type sperm than mutant sperm, most likely because the later have more mutant proteins due to continuous MIWI expression in haploid spermatids after meiosis. These data suggest that MIWI functions in a dosage-dependent manner.

### MIWI Regulates the Histone-to-Protamine Transition

Histones are long known to be gradually replaced by protamines during spermiogenesis. An initial step in histone-to-protamine exchange is histone ubiquitination, which facilitates histone removal by loosening the compact nucleosome (Rathke et al., 2014). Our study has now uncovered an unexpected role of MIWI in controlling this initial step: MIWI sequestrates RNF8, a key E3 ligase for histone ubiquitination in the cytoplasm of earlier stage spermatids, and MIWI degradation by APC/C in late spermatids releases RNF8 into the nucleus to mediate histone ubiquitination and subsequent histone-to-protamine

exchange. Our *Miwi*$^{+/DB}$-*Cre* mice phenocopy the RNF8 knockout mice in essentially all aspects, including substantial reduction of histone ubiquitination in late spermatids and severe histone retention in sperm. More importantly, our rescue strategy based on a RNF8 fragment, which impairs the interaction between endogenous RNF8 and MIWI, provides direct evidence for cytoplasmic sequestration of RNF8 by MIWI as a key disease event. Notably, RNF8-dependent histone ubiquitination was also known to establish active epigenetic modifications during meiosis and subsequently facilitate a selective set of genes from inactive sex chromosomes to avoid silencing and maintain the activation state in post-meiotic spermatids (Sin et al., 2012). It will be interesting to determine whether MIWI sequestration of RNF8 is linked to additional roles of RNF8 in epigenetic programming in future studies. Moreover, we found that MIWI significantly suppresses the ubiquitin ligase activity of RNF8 in vitro, which is independent of piRNAs and the slicer activity of the MIWI protein. This was further confirmed with a double D-box/piRNA-loading mutant MIWI by mouse testes transduction (data not shown). Additionally, unlike the observation in *shMiwi*: GFP-transfected round spermatids, we found a more diffuse RNF8 staining in *Miwi* null round spermatids but no significant nuclear translocation of RNF8 in these cells (data not shown). Given that *Miwi* null mice display spermatogenic arrest at the beginning of the round spermatid stage (Deng and Lin, 2002), it is possible that RNF8 might be controlled by another regulator(s) in an earlier stage(s) of round spermatids. Alternatively, the severe defects in *Miwi* null round spermatids may indirectly cause the dysregulation of RNF8 distribution in spermatids.

### Tracking Spermatids-to-Sperm Transformation In Vivo

Due to the complexity of spermiogenesis and the lack of an adequate in vitro cell culture system, the molecular events in this dramatic differentiation process have remained largely unclear. In our previous studies (Zhao et al., 2013; Gou et al., 2014), we developed the lentiviral testis transduction system to manipulate gene expression in spermatids as a tool for studying piRNA/Piwi function in mouse spermatid development. However, because ectopic EGFP protein expressed by lentiviral vectors is discarded during cytoplasm ejection before sperm formation, it has been technically difficult to track transduced sperm in epididymis. In our current study, we developed a new strategy by expressing an EGFP protein fused to a strong mitochondrial localization signal Cyto IV. Because mitochondria are translocated to the tails of sperm rather than disposed during cytoplasm ejection, this strategy enabled us to use EGFP to visualize the sperm developed from transduced spermatids. This strategy is generally applicable to studying other critical spermiogenic genes to advance our understanding of male germ cell development.

## Star★Methods

### Contact For Reagent and Resource Sharing

Further information and requests for resources and reagents should be directed to and will be fulfilled by the Lead Contact, Mo-Fang Liu (mfliu@sibcb.ac.cn).

## Experimental Model and Subject Details

**Human Samples—**The studies involving human subjects were approved by the Medical Ethics Review Board of hospitals and with written informed consent from the patients or their relatives. 413 patients with idiopathic azoospermia (no sperm in the ejaculate even after centrifugation) and 300 fertile male controls were recruited from the Infertility Clinic affiliated to Shanghai Institute of Planned Parenthood Research. All patients underwent semen analyses at least on three different occasions, and those with a history of orchitis, obstruction of vas deferens or endocrine disorders were excluded. All the control men had fathered at least one child. The genomic DNA was prepared from the blood samples. For the 3 patients identified with *Hiwi* D-box mutations, we further obtained their testicular biopsies and confirmed their mutations in testicular genomic DNA and cDNA.

**Mice—**All animal studies were approved by the SIBCB Institutional Animal Care and Research Advisory Committee. *Miwi* D-box mutation conditional knockin mouse model was created by Beijing Biocytogen (Beijing, China). Briefly, a loxP-flanked cassette containing the mouse *Miwi* cDNA including exons 6 to 22, the mouse *Miwi* 3′UTR sequences, and 3 × Stop-Neo sequence was placed 5′ of exon 6. Southern blot with two independent *Miwi* probes and XbaI-digested genomic DNA from different ES cell clones confirmed proper integration into the targeted locus. Two correctly targeted ES clones were injected into C57/BL6 (B6) blastocysts to generate $Miwi^{+/DB}$ mice. Southern blot were performed to identify the presence of recombined loci in targeted mice (Figure S2A). A single 16.2 kb fragment detected by both probes shows the wild-type allele, while an additional 9.4 kb fragment detected by 5′ probe and 6.9 kb fragment detected by 3′ probe indicate the successfully targeted allele (termed as $Miwi^{+/DB}$). To obtain germline-specific R218A/L221A mutation knockin mice [TNAP-Cre; $Miwi^{+/DB}$], we crossed $Miwi^{+/DB}$ miceto TNAP-Cre mice (Lomelí et al., 2000). Transgenic mice were generated by pronuclear injection (Ittner and Götz, 2007). To obtain zygotes for pronuclear injection, superovulated C57BL/6J female mice were mated with C57BL/6J males. The linearized DNA constructs were injected into the male pronucleus of fertilized oocytes. Ten to twenty embryos were transferred into each pseudopregnant ICR female. The offspring were screened for transgenic mouse lines.

## Method Details

**Immunoprecipitation and Immunoblotting—**For immunoprecipitation and immunoblotting assays, mouse spermatogenic cells were homogenized in lysis buffer [50 mM Tris-HCl (pH 7.4), 1% Triton X-100,150 mM NaCl, 5 mM EDTA, 1 × Complete Mini, proteinase Inhibitor cocktail (Roche)]. Primary antibody-coupled Protein A/G beads were added to the precleared cell lysate and incubated for 4-6 hr at 4°C. After washing the beads with washing buffer [50 mM Tris-HCl (pH 7.4), 0.1% Triton X-100, 500 mM NaCl, 5 mM EDTA, proteinase inhibitor cocktail], IP pellets and extracts of cells were diluted in SDS loading buffer and analyzed by standard SDS-PAGE and IB procedures. The band intensities in immunoblotting were quantified with an LAS4000 Image Analyzer.

**Immunostaining, Histological, Electron Microscopy, and Apoptosis Assays—**For immunostaining, testicular sections or cells were fixed with 4% paraformaldehyde,

permeabilized with 0.5% Triton X-100 in PBS, and incubated with primary antibodies and Alexa Fluor 488 or Cy3-conjugated secondary antibodies. Nuclei were counterstained with DAPI (Vector Laboratories). Laser confocal scanning images were captured with a Leica TCS SP5 inverted spectral confocal microscope. Immunostaining density was quantified using ImageJ software. For histological assay, the paraffin sections and cryo-sections of testes and epididymides were prepared as described previously (Russell et al., 1990). For Hematoxylin and Eosin (H&E) staining, 5 mm Paraffin-embedded sections of testes and epididymides were prepared and then stained with Hematoxylin and Eosin. Stages of seminiferous epithelium cycle and steps of spermatid development were determined as described previously (Russell et al., 1990). For scanning electron microscopy of sperm, cauda epididymides were dissected and minced in 0.1 M phosphate buffer (pH 7.4), allowing sperm released into the supernatant. The sperm were then fixed in 2.5% glutaraldehyde solution in phosphate buffer, collected on poly-L-lysinecoated glass coverslips, post-fixed in osmium tetroxide, dehydrated in a graded ethanol series, subjected to critical point drying and then coated with gold/palladium. Samples were examined with a SEM (FEI Quanta250). For transmission electron microscopy, cauda epididymis sections were fixed in 4% paraformaldehyde containing 0.05% glutaraldehyde in 0.1 M phosphate buffer, and then post-fixed in 1% osmium tetroxide. Dehydration was carried out in ethanol and the samples were embedded in Epon 812. Ultrathin sections were counterstained with uranyl acetate and lead citrate, and examined with a TEM (FEI Tecnai G2 Spirit). Apoptosis analysis was performed using In Situ Cell Death Detection Kit, TMR red (Roche).

**Aniline Staining—**Acidic aniline staining was performed as previously described (Roux et al., 2004) to determine the chromatin compaction of sperm nuclei. In brief, sperm from cauda epididymis were harvested, spread on slides and air-dried. Samples were fixed in 4% PFA for 30 min and washed with PBS, then treated with 0.2% Triton X-100 for 15 min. Slides were stained using acidic aniline blue staining (5% methyl blue in 100 ml 4% acetic acid) for 10 min.

**IVF and ICSI—**In vitro fertilization (IVF) was preformed according to protocol from Jackson Laboratory (http://cryo.jax.org/ivf.html). In brief, ovarian stimulation was performed using standard gonadotropin-releasing hormone agonist downregulation and gonadotropin stimulation of the ovaries. Oocytes were obtained using ultrasound-guided, transvaginal aspiration, and incubated in human tubal fluid culture medium supplemented with 15% heat-deactivated maternal sera for 4 hr prior to sperm insemination. Insemination and culture were performed using standard “microdrop” techniques. Transfer of 2-3 embryos was performed 72 hr after oocyte retrieval. Intracytoplasmic sperm injection (ICSI) was performed in cases in which the sperm penetration assay was diminished (< 15% penetration) in both the standard and refrigerated aliquots of evaluated samples. ICSI was performed using standard techniques at 4 hr after oocyte retrieval.

**Isolation of Mouse Spermatogenic Cells—**Mouse round spermatids, elongating spermatids and late spermatids (consisting of elongating and elongated spermatids) were isolated as we recently described (Zhao et al., 2013; Gou et al., 2014). In brief, mouse spermatogenic cells were extracted from the seminiferous tubules of adult ICR male mice,

and round spermatids and late spermatids were separated through the unit gravity sedimentation procedure. To isolate elongating spermatids from elongated spermatids, the elongating/elongated spermatids suspensions were incubated in a staining solution [3 mg/ml DNase I (Fermentas), 5 μg/ml Hoechst 33342 (Acros Organics), 2 μg/ml propidium iodine (Sigma)] for 30 min at 33°C, then filtered through two stacked GBSS wetted 40 mm strainers (Fisher) to remove small clumps and debris for fluorescence-activated cell sorting (FACS). The two types of spermatids showed distinguished forward scatter parameter (FSC), which allows the separation of them in two subpopulations. The $FSC^{high}$ and $FSC^{low}$ populations respectively represent elongating spermatids and elongated spermatids. The isolated spermatogenic cells were all confirmed by their distinct nuclear morphology (DAPI staining of nuclei).

**Lentivirus Packaging and Testis Transduction—**The lentiviral vectors for expressing Myc-tagged RNF8-N-IRES-Cyto-fused EGFP and its mutant were constructed as we described previously (Zhao et al., 2013). The vectors contain ~0.6 kb of *protamine 1* promoter (*Prm1*) sequence 5′ to the Myc-tagged RNF8-N (1-210 aa of RNF8) or its mutant $RNF8\text{-}N^{mut}$ ($^{68}$QNPEG$^{72}$ with $^{68}$AAAAA$^{72}$), followed with Cyto-EGFP (a mitochondrial targeting signal (Cyto) fused EGFP) linked by IRES (Figure S7E). The lentiviral vectors were packaged into pseudovirus with their cognate packaging plasmids following standard procedures. The viral supernatant was centrifuged at 50,000 × g for 90 min at 4°C for preparing high-titer lentivirus (> $10^8$ transduction units/ml). Testis transduction was performed in 5-week-old ICR male mice and carried out as we described previously (Zhao et al., 2013). In brief, the testes of pentobarbital-sodium-anesthetized mouse were pulled out, and under a microscope, ~20 μl of fresh high-titer lentivirus (no freezing and thawing) were injected into seminiferous tubules through efferent duct using a sharp glass capillary with a tip diameter of 50 μm. Abdominal wall and skin were closed with sutures after testes were carefully returned to abdominal cavities. The testes were harvested 4-5 weeks posttransduction of ectopic protein expression vectors.

**In Vitro RNF8-Histone Ubiquitination Assays—**In vitro RNF8-histone ubiquitination assays were performed as described previously (Mailand et al., 2007). ~1 μg of histone H2B (New England Biolabs) was incubated in 30 μl reaction mixture containing 50 mM Tris, pH 7.5; 5 mM MgCl2; 2 mM NaF; 2 mM ATP; 10 mM Okadaic acid; 1mMDTT; 0.1 μg E1; 0.2 μg UbcH5c; and 1 μg HA-ubiquitin (all from Boston Biochem). ~200 ng of bacterially expressed and purified GST-RNF8 was added and reactions were incubated at 37°C for 1 hr before stopped by addition of SDS-PAGE loading buffer. Flag-MIWI and Flag-MILI proteins were immune-purified with anti-Flag beads (M2 beads; Sigma) from transfected 293T cells, eluted with 3×Flag peptide, and then loaded onto a Sephadex G-75 column to remove small peptides. Then different amounts (~0.2 μg, ~0.5 μg, and ~1 μg) of purified Flag-MIWI, Flag-MIWI D-box mutant or Flag-MILI proteins were added into the ubiquitination reactions, respectively.

**Sperm Proteomic Analysis—**Sperm for proteomic analysis was obtained from ~3 month-old mice, and subjected to LC-MS/MS analysis with standard protocol. In brief, cauda epididymides were obtained from ~3 month-old mice, and placed into 2.0 ml

eppendorf tube containing 500 ml of warm Whittens-HEPES medium (pH 7.2-7.4). The tissues were gently sheared and incubated at 37°C for 30 min to allow sperm to diffuse into the medium. Then, spermatozoa were gently filtered on ice through fine nylon mesh to remove tissue debris. Next, the sperm-containing filtrate was transferred into a clean 1.5 ml eppendorf tube and spun at 500 g ×10 min at 4°C to collect sperm. The obtained sperm sample was then subjected to LC-MS/MS analysis with standard protocol for proteomic analysis.

**MIWI and RNF8 Complex Purification—**Mouse haploid spermatids were isolated through FACS modified from the procedure described previously (Gou et al., 2014). The isolated spermatids were homogenized in lysis buffer [50 mM Tris-HCl (pH 7.4), 1% Triton X-100, 150 mM NaCl, 5 mM EDTA, 1 × Complete Mini, proteinase Inhibitor cocktail (Roche)]. The extract was centrifuged at 10,000 g, 4°C, 10min. Anti-MIWI or anti-RNF8 coupled Protein A/G beads were added to the precleared cell lysate and incubated for 4-6 hr at 4°C. After washing the beads with washing buffer [50 mM Tris-HCl (pH 7.4), 0.1% Triton X-100, 500 mM NaCl, 5 mM EDTA, and proteinase inhibitor cocktail], IP pellets were subjected to on-bead trypsin digestion followed by LC-MS/MS analysis of the released peptides (Hubner et al., 2010; von Thun et al., 2013). We used software MaxQuant to filter the data and provided all identified proteins as well as their peptide number in Table S3. Specificity of the identified proteins was determined by control purifications with protein A/G coupled to rabbit IgG.

**Sperm Mobility Assays—**Sperm was harvested by dissecting cauda epididymides in 37°C pre-warmed Enriched Krebs-Ringer bicarbonate medium (EKRB medium; 120.1 mM NaCl, 4.8 mM KCl, 25.2 mM NaHCO3, 1.2 mM KH2PO4, 1.2 mM MgSO4, 1.3 mM CaCl2, supplemented with 11.1 mM glucose, 2 mM glutamine, 1 × essential amino acids, 1 × nonessential amino acids, 100 μg/ml streptomycin, 100 U/ml penicillin). ~1 μl sperm-containing medium was dropped into the calibrated slide for veterinary semen analysis (Leja) and observed by fluorescent microscopy. The movies were first shot under bright imaging and then under GFP imaging, with 50 frames per second.

### Quantification and Statistical Analysis

Student's t test was performed to compare the differences between treated groups relative to their paired controls. All results were presented as the mean ± SD and *p*-values of < 0.05 or below were considered significant.

## Supplementary Material

Refer to Web version on PubMed Central for supplementary material.

## Acknowledgments

We thank Duojia Pan and Yonggang Zheng from UT Southwestern and members of the M.-F.L. and H.-J.S. laboratories for helpful comments; Guoliang Xu (SIBCB) for TNAP-Cre mice; Hu Zhou and Jing Gao from SIMM, Yonglian Zhang, Minghan Tong, Gang Wang, Ronggui Hu, Wei Tang, Bang-An Wang, and Xiao Yao from SIBCB, Shunmin He, Peng Zhang, and Fei Gao from IOZ, Qinghua Shi (USTC), Feng Zhang (Fudan), and Zhimin Huang (SJTU) for experimental assistance. This work was supported by grants from the Chinese Academy of Sciences (“Strategic Priority Research Program” grants XDB19010203), National Natural Science Foundation of China

(31325008, 91640201 and 81671512), Ministry of Science and Technology of China (2017YFA0504400, 2014CB943100 and 2014CB964800), Science and Technology Commission of Shanghai Municipality (13ZR1464300 and 16XD1404900), and the Foundation of Key Laboratory of Gene Engineering of the Ministry of Education. L.-T.G. and X.-D.F. were supported by the NIH (grants GM052872 and HG004659).

## References

Balhorn R. The protamine family of sperm nuclear proteins. Genome Biol. 2007; 8:227. [PubMed: 17903313]

Barckmann B, Pierson S, Dufourt J, Papin C, Armenise C, Port F, Grentzinger T, Chambeyron S, Baronian G, Desvignes JP, et al. Aubergine iCLIP reveals piRNA-dependent decay of mRNAs involved in germ cell development in the early embryo. Cell Rep. 2015; 12:1205–1216. [PubMed: 26257181]

Batista PJ, Ruby JG, Claycomb JM, Chiang R, Fahlgren N, Kasschau KD, Chaves DA, Gu W, Vasale JJ, Duan S, et al. PRG-1 and 21U-RNAs interact to form the piRNA complex required for fertility in C. elegans. Mol Cell. 2008; 31:67–78. [PubMed: 18571452]

Braun RE. Packaging paternal chromosomes with protamine. Nat Genet. 2001; 28:10–12. [PubMed: 11326265]

Carmell MA, Girard A, van de Kant HJ, Bourc'his D, Bestor TH, de Rooij DG, Hannon GJ. MIWI2 is essential for spermatogenesis and repression of transposons in the mouse male germline. Dev Cell. 2007; 12:503–514. [PubMed: 17395546]

Cora E, Pandey RR, Xiol J, Taylor J, Sachidanandam R, McCarthy AA, Pillai RS. The MID-PIWI module of Piwi proteins specifies nucleotide- and strand-biases of piRNAs. RNA. 2014; 20:773–781. [PubMed: 24757166]

Cox DN, Chao A, Baker J, Chang L, Qiao D, Lin H. A novel class of evolutionarily conserved genes defined by piwi are essential for stem cell self-renewal. Genes Dev. 1998; 12:3715–3727. [PubMed: 9851978]

De Fazio S, Bartonicek N, Di Giacomo M, Abreu-Goodger C, Sankar A, Funaya C, Antony C, Moreira PN, Enright AJ, O'Carroll D. The endonuclease activity of Mili fuels piRNA amplification that silences LINE1 elements. Nature. 2011; 480:259–263. [PubMed: 22020280]

Deng W, Lin H. miwi, a murine homolog of piwi, encodes a cytoplasmic protein essential for spermatogenesis. Dev Cell. 2002; 2:819–830. [PubMed: 12062093]

Ferlin A, Arredi B, Foresta C. Genetic causes of male infertility. Reprod Toxicol. 2006; 22:133–141. [PubMed: 16806807]

Gou LT, Dai P, Yang JH, Xue Y, Hu YP, Zhou Y, Kang JY, Wang X, Li H, Hua MM, et al. Pachytene piRNAs instruct massive mRNA elimination during late spermiogenesis. Cell Res. 2014; 24:680–700. [PubMed: 24787618]

Gu A, Ji G, Shi X, Long Y, Xia Y, Song L, Wang S, Wang X. Genetic variants in Piwi-interacting RNA pathway genes confer susceptibility to spermatogenic failure in a Chinese population. Hum Reprod. 2010; 25:2955–2961. [PubMed: 20940137]

Han BW, Wang W, Li C, Weng Z, Zamore PD. Noncoding RNA. piRNA-guided transposon cleavage initiates Zucchini-dependent, phased piRNA productionz. Science. 2015; 348:817–821. [PubMed: 25977554]

Harris AN, Macdonald PM. Aubergine encodes a Drosophila polar granule component required for pole cell formation and related to eIF2C. Development. 2001; 128:2823–2832. [PubMed: 11526087]

Houwing S, Berezikov E, Ketting RF. Zili is required for germ cell differentiation and meiosis in zebrafish. EMBO J. 2008; 27:2702–2711. [PubMed: 18833190]

Hu Z, Xia Y, Guo X, Dai J, Li H, Hu H, Jiang Y, Lu F, Wu Y, Yang X, et al. A genome-wide association study in Chinese men identifies three risk loci for non-obstructive azoospermia. Nat Genet. 2012; 44:183–186.

Hubner NC, Bird AW, Cox J, Splettstoesser B, Bandilla P, Poser I, Hyman A, Mann M. Quantitative proteomics combined with BAC TransgeneOmics reveals in vivo protein interactions. J Cell Biol. 2010; 189:739–754. [PubMed: 20479470]

Ittner LM, Götz J. Pronuclear injection for the production of transgenic mice. Nat Protoc. 2007; 2:1206–1215. [PubMed: 17546016]

Iwasaki YW, Siomi MC, Siomi H. PIWI-interacting RNA: its biogenesis and functions. Annu Rev Biochem. 2015; 84:405–433. [PubMed: 25747396]

Izumi N, Shoji K, Sakaguchi Y, Honda S, Kirino Y, Suzuki T, Katsuma S, Tomari Y. Identification and functional analysis of the pre-piRNA 3′ Trimmer in silkworms. Cell. 2016; 164:962–973. [PubMed: 26919431]

Juliano C, Wang J, Lin H. Uniting germline and stem cells: the function of Piwi proteins and the piRNA pathway in diverse organisms. Annu Rev Genet. 2011; 45:447–469. [PubMed: 21942366]

Kornberg RD, Thomas JO. Chromatin structure; oligomers of the histones. Science. 1974; 184:865–868. [PubMed: 4825888]

Kuramochi-Miyagawa S, Kimura T, Ijiri TW, Isobe T, Asada N, Fujita Y, Ikawa M, Iwai N, Okabe M, Deng W, et al. Mili, a mammalian member of piwi family gene, is essential for spermatogenesis. Development. 2004; 131:839–849. [PubMed: 14736746]

Lomelí H, Ramos-Mejía V, Gertsenstein M, Lobe CG, Nagy A. Targeted insertion of Cre recombinase into the TNAP gene: excision in primordial germ cells. Genesis. 2000; 26:116–117. [PubMed: 10686602]

Lu LY, Wu J, Ye L, Gavrilina GB, Saunders TL, Yu X. RNF8-dependent histone modifications regulate nucleosome removal during spermatogenesis. Dev Cell. 2010; 18:371–384. [PubMed: 20153262]

Mailand N, Bekker-Jensen S, Faustrup H, Melander F, Bartek J, Lukas C, Lukas J. RNF8 ubiquitylates histones at DNA double-strand breaks and promotes assembly of repair proteins. Cell. 2007; 131:887–900. [PubMed: 18001824]

Meister G. Argonaute proteins: functional insights and emerging roles. Nat Rev Genet. 2013; 14:447–459. [PubMed: 23732335]

Meistrich ML, Mohapatra B, Shirley CR, Zhao M. Roles of transition nuclear proteins in spermiogenesis. Chromosoma. 2003; 111:483–488. [PubMed: 12743712]

Mohn F, Handler D, Brennecke J. Noncoding RNA. piRNA-guided slicing specifies transcripts for Zucchini-dependent, phased piRNA biogenesis. Science. 2015; 348:812–817. [PubMed: 25977553]

Oliva R. Protamines and male infertility. Hum Reprod Update. 2006; 12:417–435. [PubMed: 16581810]

Rathke C, Baarends WM, Awe S, Renkawitz-Pohl R. Chromatin dynamics during spermiogenesis. Biochim Biophys Acta. 2014; 1839:155–168. [PubMed: 24091090]

Reuter M, Berninger P, Chuma S, Shah H, Hosokawa M, Funaya C, Antony C, Sachidanandam R, Pillai RS. Miwi catalysis is required for piRNA amplification-independent LINE1 transposon silencing. Nature. 2011; 480:264–267. [PubMed: 22121019]

Roux C, Tripogney C, Joanne C, Bresson JL. Nuclear quality of the spermatozoon: exploration tests of the chromatin of human spermatozoa (nuclear proteins). Gynecol Obstet Fertil. 2004; 32:792–798. [PubMed: 15380764]

Russell LD, Weiss T, Goh JC, Curl JL. The effect of subman-dibular gland removal on testicular and epididymal parameters. Tissue Cell. 1990; 22:263–268. [PubMed: 2237906]

Sasaki T, Shiohama A, Minoshima S, Shimizu N. Identification of eight members of the Argonaute family in the human genome. Genomics. 2003; 82:323–330. [PubMed: 12906857]

Schultz N, Hamra FK, Garbers DL. A multitude of genes expressed solely in meiotic or postmeiotic spermatogenic cells offers a myriad of contraceptive targets. Proc Natl Acad Sci USA. 2003; 100:12201–12206. [PubMed: 14526100]

Sin HS, Barski A, Zhang F, Kartashov AV, Nussenzweig A, Chen J, Andreassen PR, Namekawa SH. RNF8 regulates active epigenetic modifications and escape gene activation from inactive sex chromosomes in post-meiotic spermatids. Genes Dev. 2012; 26:2737–2748. [PubMed: 23249736]

Siomi MC, Sato K, Pezic D, Aravin AA. PIWI-interacting small RNAs: the vanguard of genome defence. Nat Rev Mol Cell Biol. 2011; 12:246–258. [PubMed: 21427766]

Tang W, Tu S, Lee HC, Weng Z, Mello CC. The RNase PARN-1 trims piRNA 3′ ends to promote transcriptome surveillance in C. elegans. Cell. 2016; 164:974–984. [PubMed: 26919432]

von Thun A, Preisinger C, Rath O, Schwarz JP, Ward C, Monsefi N, Rodríguez J, Garcia-Munoz A, Birtwistle M, Bienvenut W, et al. Extracellular signal-regulated kinase regulates RhoA activation and tumor cell plasticity by inhibiting guanine exchange factor H1 activity. Mol Cell Biol. 2013; 33:4526–4537. [PubMed: 24043311]

Vourekas A, Alexiou P, Vrettos N, Maragkakis M, Mourelatos Z. Sequence-dependent but not sequence-specific piRNA adhesion traps mRNAs to the germ plasm. Nature. 2016; 531:390–394. [PubMed: 26950602]

Wang XN, Li ZS, Ren Y, Jiang T, Wang YQ, Chen M, Zhang J, Hao JX, Wang YB, Sha RN, et al. The Wilms tumor gene, Wt1, is critical for mouse spermatogenesis via regulation of sertoli cell polarity and is associated with non-obstructive azoospermia in humans. PLoS Genet. 2013; 9:e1003645. [PubMed: 23935527]

Watanabe T, Cheng EC, Zhong M, Lin H. Retrotransposons and pseudogenes regulate mRNAs and lncRNAs via the piRNA pathway in the germline. Genome Res. 2015; 25:368–380. [PubMed: 25480952]

Yan W. Male infertility caused by spermiogenic defects: lessons from gene knockouts. Mol Cell Endocrinol. 2009; 306:24–32. [PubMed: 19481682]

Yu Y, Gu J, Jin Y, Luo Y, Preall JB, Ma J, Czech B, Hannon GJ. Panoramix enforces piRNA-dependent cotranscriptional silencing. Science. 2015; 350:339–342. [PubMed: 26472911]

Zhang P, Kang JY, Gou LT, Wang J, Xue Y, Skogerboe G, Dai P, Huang DW, Chen R, Fu XD, et al. MIWI and piRNA-mediated cleavage of messenger RNAs in mouse testes. Cell Res. 2015; 25:193–207. [PubMed: 25582079]

Zhao S, Gou LT, Zhang M, Zu LD, Hua MM, Hua Y, Shi HJ, Li Y, Li J, Li D, et al. piRNA-triggered MIWI ubiquitination and removal by APC/C in late spermatogenesis. Dev Cell. 2013; 24:13–25. [PubMed: 23328397]

## Highlights

- *Hiwi* ubiquitination-deficient D-box mutations are detected in azoospermia patients
- D-box mutant knockin mice display spermatogenic failure at late spermiogenesis
- Stabilized MIWI ties RNF8 up in the cytoplasm to prevent histone ubiquitination
- Blocking MIWI-RNF8 interaction functionally rescues defective spermiogenesis

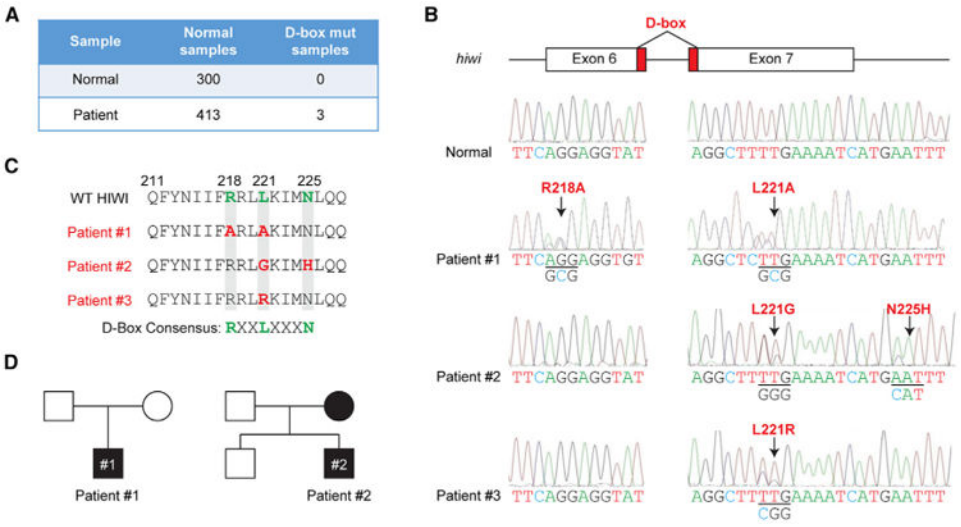


**Figure 1. Identification of D-Box Mutations in *hiwi* Genes from Patients with Azoospermia**

(A) A total of 413 patients with azoospermia and 300 fertile controls analyzed in this study.

(B) Chromatogram of the sequences of *Hiwi* D-box element-encoding region spanning sixth and seventh exons in one fertile control and three patients with azoospermia.

(C) Comparison of the wild-type and mutated D-box elements in HIWI proteins.

(D) Pedigrees of Patients 1 and 2 for their D-box mutations.

See also Figure S1.

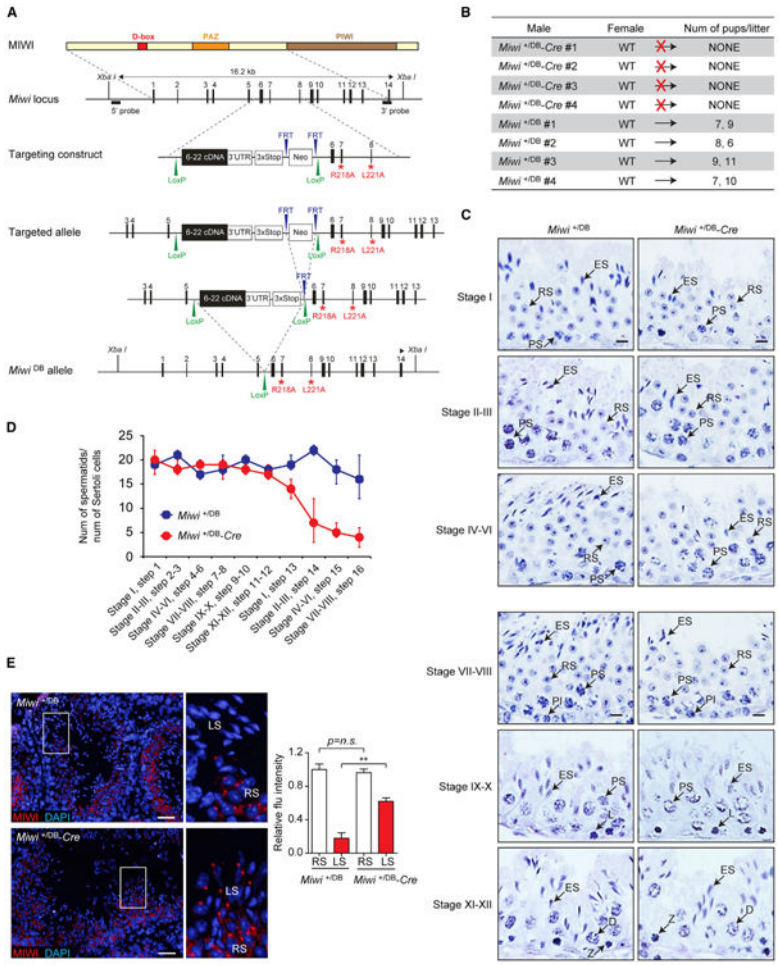


**Figure 2. *Miwi* D-Box Mutation Knockin Mice Show Male Sterility**

(A) A schematic diagram illustrating the construction of conditional knockin of the D-box mutations (R218A/L221A) in *Miwi* (*Miwi*$^{DB}$) and the generation of *Miwi*$^{DB}$ allele by Cre-mediated recombination.

(B) All tested *Miwi*$^{+/DB}$-*Cre* males were infertile.

(C) H&E staining of testis sections from dpp 12-week mice. Stages of seminiferous epithelium cycles were determined by morphology of spermatocytes and round spermatids. Pl, preleptotene; L, leptotene; Z, zygotene; P, pachytene; D, diplotene; RS, round spermatids; ES, elongating spermatids. Scale bar, 20 μm.

(D) Late spermatids were reduced in *Miwi*$^{+/DB}$-*Cre* testes. Ratios between spermatids and Sertoli cells in tubule cross sections of specific stages of seminiferous epithelial cycles and corresponding spermatid development steps were shown.

(E) Immunostaining of testis sections from dpp 12-week mice for MIWI (red) with nuclei counterstained by DAPI (blue). Left: representative staining images with an enlargement of white framed region on the right. Right: quantification of anti-MIWI staining density in round spermatids (RS, blank column) or late spermatids (LS, red column) (n = 100 per group; the average values ± SD of three separate experiments are plotted). Scale bar, 50 μm. Results shown are representative of three independent experiments. **p < 0.01.

See also Figures S2 and S3.

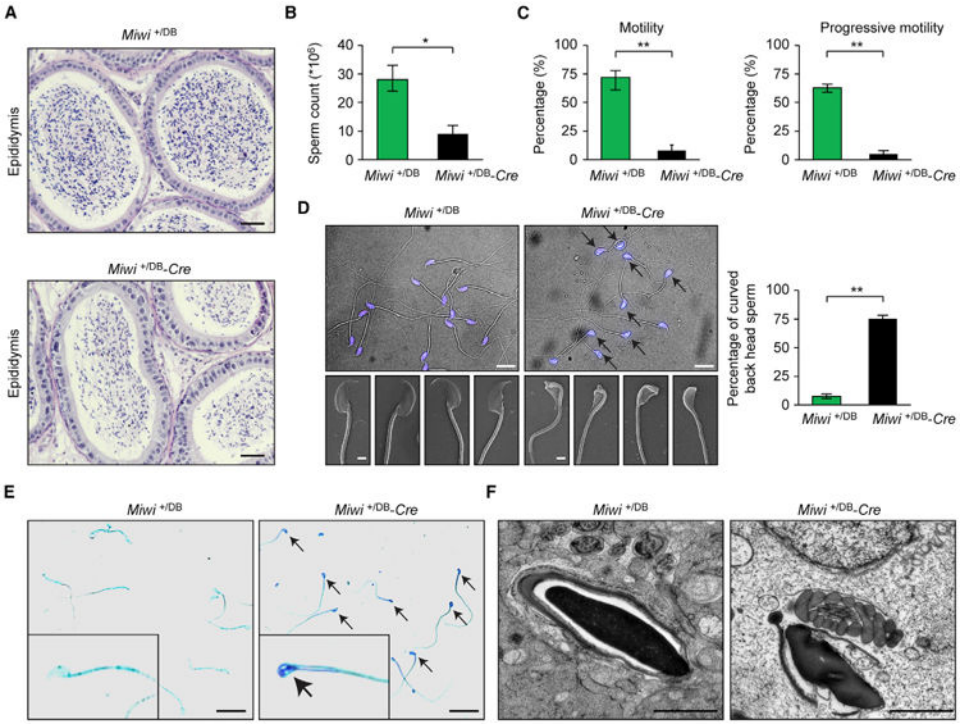


**Figure 3. Spermiogenesis Is Defective in *Miwi*$^{+/DB}$-*Cre* Mice**

(A) H&E staining of paraffin cauda epididymis sections from dpp 12-week mice. Scale bar, 50 μm.

(B) Sperm counts in cauda epididymis from dpp 12-week mice (n = 5).

(C) CASA assays of motility (left) and progressive motility (right) of sperm from 12-week mice.

(D) Sperm from *Miwi*$^{+/DB}$-*Cre* males showed abnormal morphology. Left top: representative DIC micrograph images of sperm from 12-week mice, with nuclei counterstained with DAPI (blue). Scale bar, 10 μm. Left bottom: representative scanning electron micrograph images of sperm from 12-week mice. Scale bar, 2 μm. Right: quantification of malformed sperm in *Miwi*$^{+/DB}$-*Cre* and control *Miwi*$^{+/DB}$ males (n = 100 per group; the average values ± SD of three separate experiments are plotted).

(E) Acidic Aniline staining of cauda epididymal sperm from dpp 12-week mice. The black frames indicate an enlargement of one sperm. Arrows in right panel indicate the malformed sperm. Scale bar, 20 μm. F) Representative images of transmission electron micrographs of sperm heads from dpp 12-week mice. Scale bar, 1 μm.

Results shown are representative of three independent experiments. *$p < 0.05$, **$p < 0.01$. See also Figures S2, S3, and S4 and Movie S1.

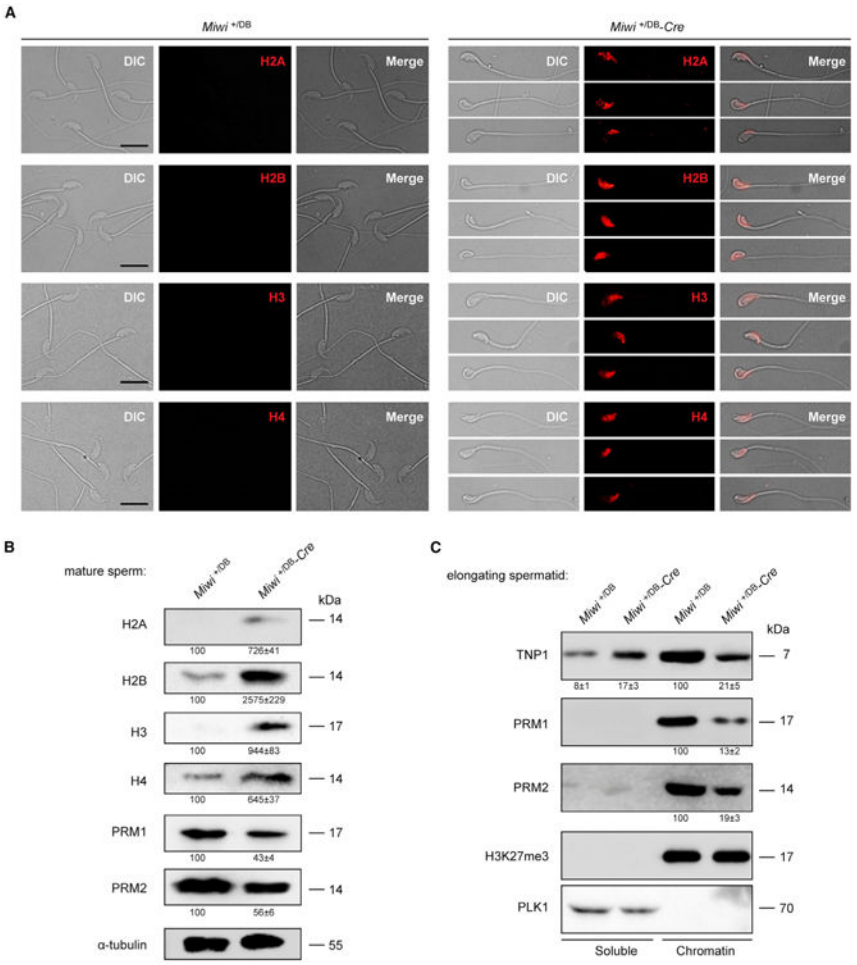


**Figure 4. The Histone-to-Protamine Exchange Is Impaired during Spermiogenesis in *Miwi*$^{+/DB}$-*Cre* Mice**

(A) Immunostaining of histones (red) in sperm from dpp 12-week mice. Representative immunostaining images with indicated histone are shown.

(B) Western blotting assays of histones and protamines in sperm from dpp 12-week mice, with α-tubulin serving as a loading control. Quantification of blotting intensity for indicated proteins is shown in parentheses (the one in control *Miwi*$^{+/DB}$ sperm is set as 100% after normalization with α-tubulin blotting).

(C) Western blotting assays of transition protein TNP1 and protamines PRM1 and PRM2 in NETN-soluble or HCl-released chromatin-bound fractions in elongating spermatids from dpp 12-week mice, with Plk1 and H3K27me3 serving as loading controls for soluble and chromatin fractions, respectively. Quantification of blotting intensity for indicated proteins is shown in parentheses (the one in *Miwi*$^{+/DB}$ control is set as 100% after normalization with H3K27me3 blotting). Results shown are representative of three independent experiments. See also Figure S4 and Tables S1 and S2.

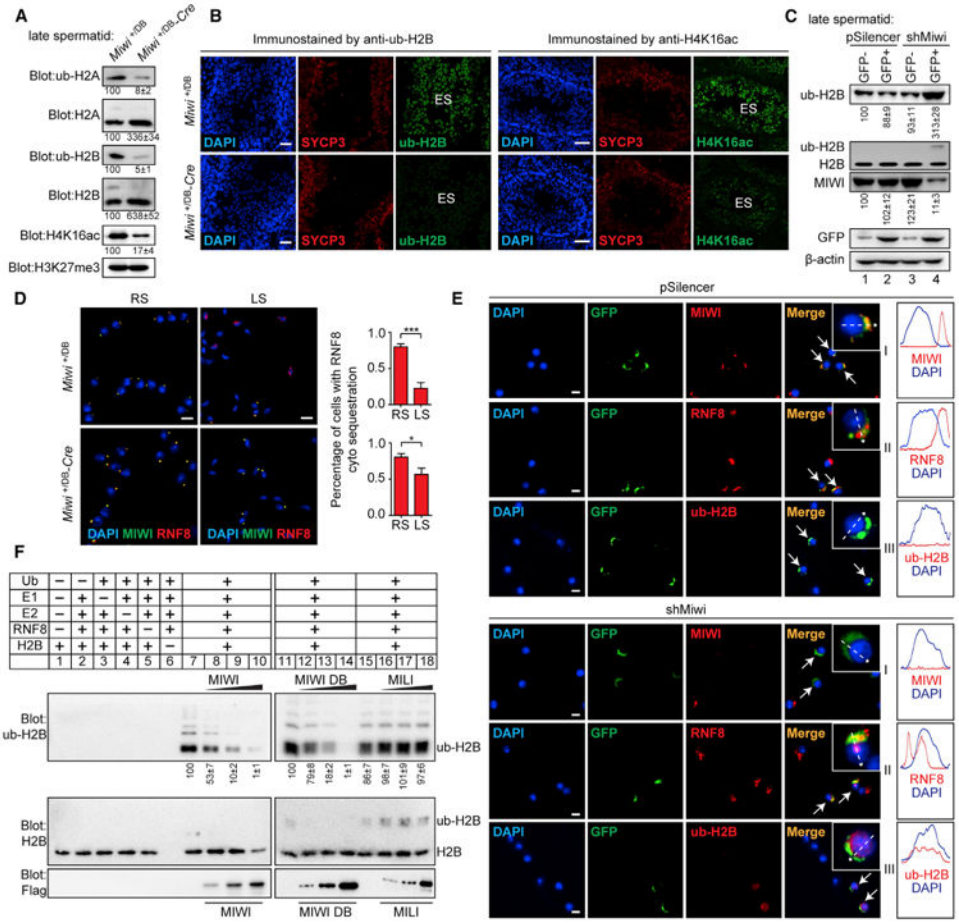


**Figure 5. MIWI Inhibits Histone Ubiquitination in Mouse Spermatids via Sequestration of RNF8**

(A) Western blotting of ub-H2A, ub-H2B, and H4K16ac in late spermatids from dpp 12-week mice with H3K27me3 as a loading control. Quantification of blotting intensity for indicated proteins is shown in parentheses (the one in *Miwi*$^{+/DB}$ control is set as 100% after normalization with H3K27me3 blotting).

(B) Immunostaining of ub-H2B (green, left) and H4K16ac (green, right) in testis sections from dpp 12-week mice with SYCP3 (red) serving as staining control. Nuclei were stained with DAPI (blue). Scale bar, 50 μm. ES, elongating spermatids.

(C) MIWI knockdown significantly enhanced ub-H2B in *Miwi*$^{+/DB}$-*Cre* late spermatids. GFP$^{-}$ and GFP$^{+}$ late spermatids were purified from shMiwi:GFP- or pSilencer:GFP-transduced testes. Quantification of blotting intensity for indicated proteins is shown in parentheses (the one in control GFP$^{-}$ late spermatids from pSilencer:GFP-transduced testes is set as 100% after normalization with β-actin blotting).

(D) Double immunostaining of MIWI (green) and RNF8 (red) in round spermatids (RS) and late spermatids (LS) from dpp 12-week mice, with nuclei counterstained by DAPI (blue). Colocalization of MIWI and RNF8 is shown in yellow. Left: representative staining images; right, quantification of round spermatids (RS) or late spermatids (LS) showing cytoplasm sequestration of RNF8 (n = 100 per group; the average values ± SD of three separate experiments are plotted). Scale bar, 10 μm.

(E) Immunostaining of MIWI (top lanes, red), RNF8 (middle lanes, red), or ub-H2B (bottom lanes, red) in round spermatids from testes transduced by pSilencer:GFP (top) or shMiwi:GFP (bottom). White framed region in right lanes of staining images, an enlargement of the representative transduced cells; right panels, areas of co-localization shown by line intensity profiles. GFP (green) and arrows indicate cells that were successfully transduced with the constructs. Nuclei were stained with DAPI (blue). Scale bar, 10 μm.

(F) Both wild-type and D-box mutant MIWI proteins inhibited RNF8-mediated H2B ubiquitination in vitro. The reactions were carried out in the absence of MIWI/MILI protein (lanes 7, 11, and 15), or in the presence of increasing amounts of wild-type Flag-MIWI (lanes 8–10), Flag-D-box mutant MIWI (lanes 12–14), or Flag-MILI proteins (lanes 16–18), with omission of one component in the reactions serving as negative controls (lanes 1–6). The Flag-tagged PIWI proteins were purified from transfected 293T cells. Quantification of blotting intensity for ub-H2B is shown in parentheses (the one in reaction without MIWI/MILI proteins [lanes 7 and 11] is set as 100%).

Results shown are representative of three independent experiments. *$p < 0.05$, ***$p < 0.001$. See also Figures S5, S6, and S7 and Table S3.

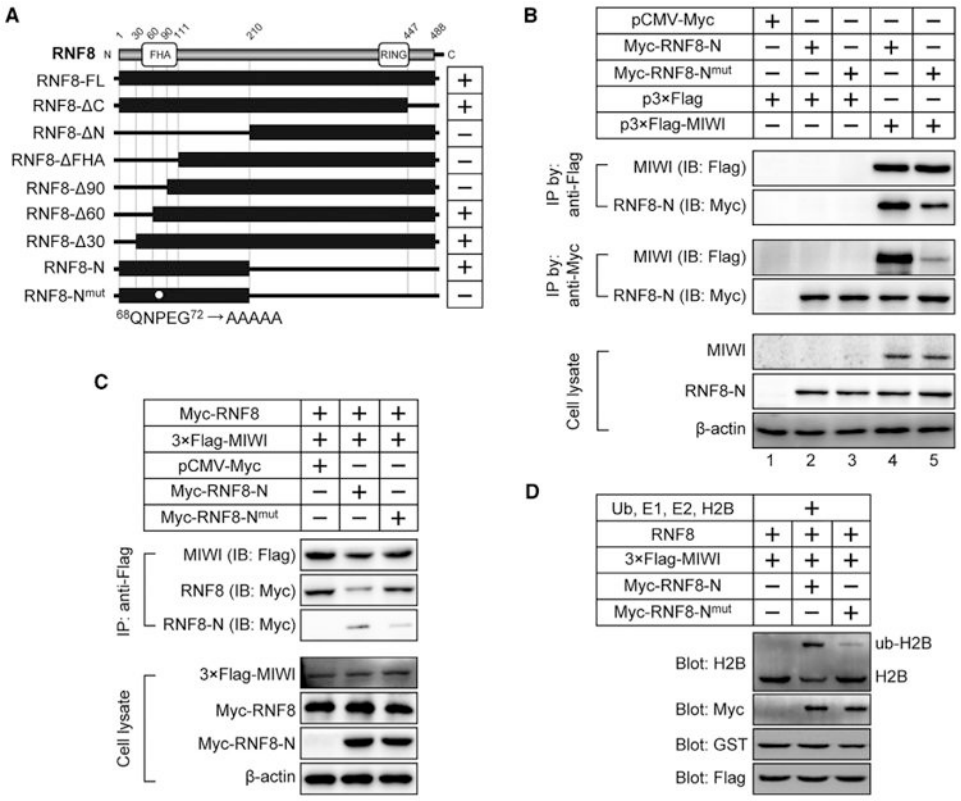


**Figure 6. RNF8 Binds to MIWI via Its $^{68}$QNPEG$^{72}$ Motif in N-Terminal Domain**

(A) Overview of a series of truncated RNF8 mutants used to map RNF8 domain(s) responsible for MIWI binding. The "+" symbol indicates binding activity retained.

(B) CoIP assays of the interaction between MIWI and RNF8-N or RNF8-N$^{mut}$ peptides in co-transfected 293T cells. Anti-Flag IP (top) and anti-Myc IP pellets (middle) were respectively immunoblotted by anti-Myc and anti-Flag antibodies. Bottom: cell lysates immunoblotted by anti-Flag or anti-Myc antibodies, with β-actin serving as a loading control.

(C) Co-IP assays of the effects of RNF8-N and RNF8-N$^{mut}$ peptides on the binding of full-length RNF8 to MIWI in co-transfected 293T cells.

(D) In vitro RNF8-mediated H2B ubiquitination assays. RNF8-N but not RNF8-N$^{mut}$ peptide relieved the inhibition of RNF8 by MIWI.

Results shown are representative of three independent experiments.

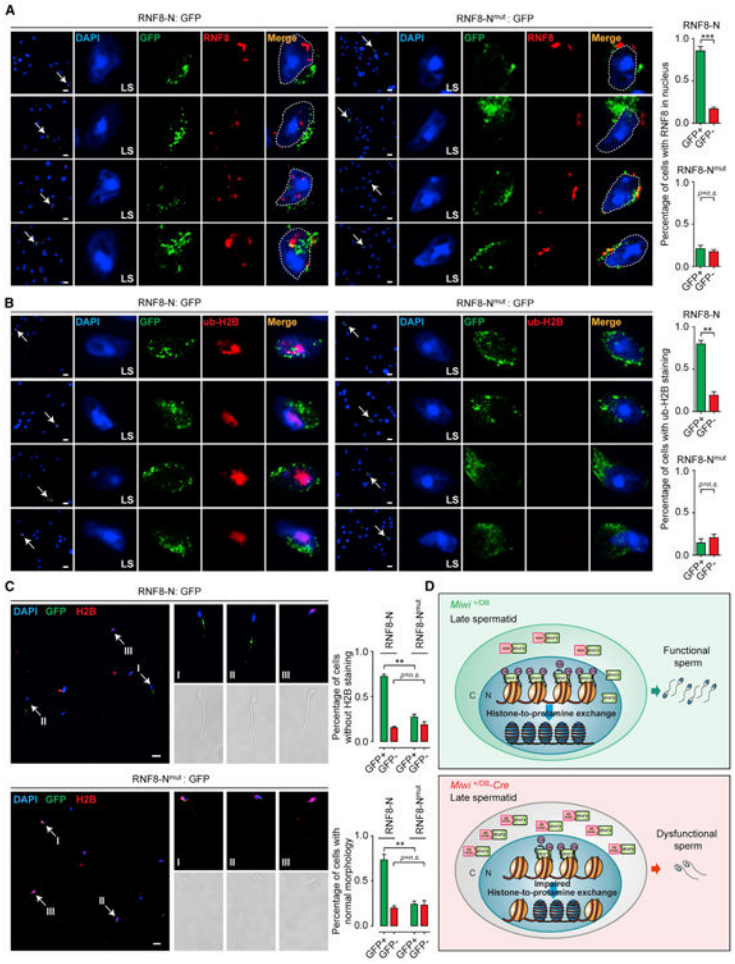


**Figure 7. The RNF8-N Peptide Effectively Rescues Defective Spermiogenesis in *Miwi*$^{+/DB}$-*Cre* Mice**

(A–C) Immunostaining of endogenous RNF8 (A), (red) or ub-H2B (B), (red) in late spermatids (LS) and H2B in sperm (C), (red) from *Miwi*$^{+/DB}$-*Cre* males transduced by RNF8-N:Cyto IV-EGFP (left) or RNF8-N$^{mut}$:Cyto IV-EGFP (right), with nuclei counterstained by DAPI (blue). Left lanes in each staining panel show the representative staining images, and GFP (green) and arrows indicate cells that were successfully transduced with the respective constructs; right lanes show an enlarged view of the representative cells. Right panels: quantification of late spermatids showing visible RNF8 nucleus translocation (A) or ub-H2B staining (B), and sperm without H2B staining (C), top) or with normal morphology (C), bottom) among GFP$^{+}$ or GFP$^{-}$ cells (n = 100 per group; the average values ± SD of three separate experiments are plotted). Scale bar, 10 μm.

(D) Schematic models showing that MIWI regulates the histone-to-protamine transition during spermiogenesis by sequestration of RNF8.

Results shown are representative of three independent experiments. **p < 0.01, ***p < 0.001.

See also Figure S7E and Movies S1, S2, and S3.

## Key Resources Table

| REAGENT or RESOURCE | SOURCE | IDENTIFIER |
|---|---|---|
| Antibodies | | |
| Mouse monoclonal anti-Myc | Sigma | Cat#M4339 |
| Mouse monoclonal anti-Flag | Sigma | Cat#F3165; RRID: AB_259529 |
| Mouse monoclonal anti-β-actin | Sigma | Cat#A3854; RRID: AB_262011 |
| Mouse monoclonal anti-Ub | Santa Cruz | sc-8017; RRID: AB_628423 |
| Rabbit polyclonal anti-H2A | Cell Signaling Technology | Cat#12349 |
| Rabbit polyclonal anti-H2B | Cell Signaling Technology | Cat#12364 |
| Rabbit polyclonal anti-H3 | Cell Signaling Technology | Cat#9715; RRID:AB_331563 |
| Rabbit polyclonal anti-H4 | Cell Signaling Technology | Cat#13919 |
| Rabbit polyclonal anti-ub-H2B | Cell Signaling Technology | Cat#5546; RRID:AB_10693452 |
| Rabbit polyclonal anti-H3K27me3 | Cell Signaling Technology | Cat#9733; RRID:AB_2616029 |
| Rabbit polyclonal anti-ub-H2A | Millipore | Cat#ABE569 |
| Rabbit polyclonal anti-RNF8 | Proteintech | Cat#14112-1-AP |
| Rabbit polyclonal anti-TNP1 | Proteintech | Cat#17178-1-AP; RRID:AB_2206757 |
| Rabbit polyclonal anti-α-tubulin | Bioworld | Cat#BS1699; RRID:AB_1664134 |
| Goat polyclonal anti-HIWI | Santa Cruz | sc-22685; RRID:AB_2165430 |
| Rabbit polyclonal anti-MIWI | Customized in ABclonal Technology (Wuhan, China) | |
| Rabbit polyclonal anti-GST | ABclonal Technology (Wuhan, China) | Cat#AE006 |
| Mouse monoclonal anti-GFP | Abways technology | Cat#AB0005 |
| Goat polyclonal anti-PRM1 | Santa Cruz | sc-23107; RRID:AB_2171310 |
| Goat polyclonal anti-PRM2 | Santa Cruz | sc-23104; RRID:AB_2284440 |
| Chemicals, Peptides, and Recombinant Proteins | | |
| Human, Recombinant Histone H2A | New England BioLabs | Cat#M2502S |
| Human, Recombinant Histone H2B | New England BioLabs | Cat#M2505S |
| Hematoxylin and Eosin | Shanghai hongqiao lexiang medical reagent technology co., LTD | N/A |
| Dynabeads protein G | Life Technologies | REF10004D |
| Critical Commercial Assays | | |
| In Situ Cell Death Detection Kit, TMR red | Roche | REF12156792910 |
| KOD-Plus-mutagenesis kit | Toyobo | Cat#SMK-101 |
| Experimental Models: Cell Lines | | |
| HEK293T | American Type Culture Collection | N/A |
| Experimental Models: Organisms/Strains | | |
| $Miwi^{+/DB}$ | This paper | N/A |
| WT/Tg | This paper | N/A |
| DB/Tg | This paper | N/A |

| REAGENT or RESOURCE | SOURCE | IDENTIFIER |
|---|---|---|
| Tnap-Cre | Nanjing Biomedical Research Institute of Nanjing University | J008569 |
| Recombinant DNA | | |
| pCMV-3 × Flag | Sigma | N/A |
| pCMV-Myc | Clontech | N/A |
| pGEX-KG | GE-Healthcare | N/A |
| pSilencer-shMiwi | This paper | N/A |
| pLV-Prm-RNF8-N-IRES-CytoIV-EGFP | This paper | N/A |
| Sequence-Based Reagents | | |
| qPCR for RNF8-F: GAACGGAGAGCAAAGAGACT | This paper | N/A |
| qPCR for RNF8-R: GCACAGACTTCCTAACTCAG | This paper | N/A |
| qPCR for GAPDH-F: TCATCATCTCCGCCCCTTCT | This paper | N/A |
| qPCR for GAPDH-R: CTGGGTGGCAGTGATGGCAT | This paper | N/A |
| qPCR for EGFP-F: GCTGACCCTGAAGTTCATCT | This paper | N/A |
| qPCR for EGFP-R: CTTGAAGAAGATGGTGCGCT | This paper | N/A |
| sh*Miwi*: CAAGTAATCGGAAGGACAA | This paper | N/A |
| piR-1: pUGACAUGAACACAGGUGCUCAGAUAGCUUUm | This paper | N/A |
| Software and Algorithms | | |
| ImageJ | Wayne Rasband | Version1.49 |